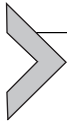

CHAPTER FOUR

Semiconductor Membrane Lasers and Photodiode on Si

Shigehisa Arai[1], Tomohiro Amemiya[1]
Institute of Innovative Research (IIR), Tokyo Institute of Technology, Tokyo, Japan
[1]Corresponding authors: e-mail address: arai@pe.titech.ac.jp; amemiya.t.ab@m.titech.ac.jp

Contents

1. Introduction 71
2. Semiconductor Membrane Lasers for Low Power Operation 74
3. Energy Cost Analysis of Membrane DR Lasers 76
4. Membrane DFB and DR Lasers on Si 79
   4.1 Fabrication Process 80
   4.2 Static Lasing Properties 82
   4.3 Direct Modulation Properties 84
5. Membrane PD on Si 86
6. Integrated Membrane DFB Laser and p-i-n PD 88
7. Summary 91
References 91

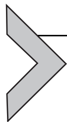

1. INTRODUCTION

GaInAsP/InP long-wavelength (1.5–1.6 μm) lasers have been widely used in long-distance optical fiber communications and monolithic integration of these lasers with other functional devices such as electroabsorption modulators and/or monitoring photodiodes (PDs), multiple wavelength laser arrays, and wavelength tunable lasers integrated with microheaters has been widely used in practical systems. Recently, hybrid integration of many functional photonic components including active photonic devices is in progress for cost-effective production of compact photonic integrated circuits (PICs) (Heck et al., 2011, 2013). On the other hand, short-reach (a few meters to a few kilometers) optical fiber communications, which consist of a huge number (several tens of thousands to several

Semiconductors and Semimetals, Volume 99
ISSN 0080-8784
https://doi.org/10.1016/bs.semsem.2018.07.002
© 2018 Elsevier Inc.
All rights reserved.

hundreds of thousands) of semiconductor lasers, have been used in supercomputers which require huge capacity signal transmission (Doany, 2012; TSUBAME2.5, 2013).

Looking at progress in large-scale integrated circuits (LSIs), the total chip power dissipation became grossly affected by the metal wiring (Banerjee and Mehrotra, 2001; Borkar and Chien, 2011; Ho et al., 2001), and high-speed signal transmissions with an energy cost close to 0.3 pJ/bit were demonstrated in 2008 (Maekawa et al., 2008; Mensink et al., 2007). In order to solve wiring problems of future LSIs, a possibility of optical interconnects was proposed in 1980s (Goodman et al., 1984), but semiconductor lasers with low power consumption operation were not available at that time. After a demonstration of ultra-low threshold current vertical cavity surface-emitting laser (VCSEL) in 1995 (Yang et al., 1995), the possibility of semiconductor lasers for on-chip optical interconnects became more realistic (Chen et al., 2007; Miller, 2000; Ohashi et al., 2009). In 2000, it was predicted that the available energy cost to send one-bit signal would be less than 100 fJ/bit (Miller, 2000), which was much lower than the energy cost of electrical wires at that time (Rattner, 2006). In 2009, device requirements of on-chip optical interconnects became more severe because the energy cost of electrical signal transmission has been improved much (Miller, 2009).

A lot of works were reported on high-speed optical detectors, optical modulators, and light sources with high-speed and low power consumption operation. High-speed operations of Ge (Kang et al., 2009; Rouvìre et al., 2005; Vivien et al., 2009; Yin et al., 2007) and InP/InGaAs (Binetti et al., 2010) photodetectors prepared on SOI substrates were demonstrated. As for modulators based on Si, a Mach-Zehnder interferometric modulator with a 3 dB cut-off frequency higher than 30 GHz (Liao et al., 2007), a four-channel wavelength division multiplexed microring modulator with a speed of 50 Gb/s (Manipatruni et al., 2009), and a complementary metal-oxide semiconductor (CMOS) modulator with an optical pulse energy of 400 fJ/bit under a driving voltage of 1 V (Zheng et al., 2010) were demonstrated. As for light sources prepared on Si or SOI substrates, a Raman silicon laser (Rong et al., 2005, 2007) and a direct gap transition from Ge-on-Si (Liu et al., 2009, 2010) under an optical pumping were demonstrated. Room-temperature continuous-wave (RT-CW) operations of injection-type III–V semiconductor lasers prepared on Si substrates were demonstrated by a wafer direct bonding method (Wada and Kamijoh, 1996), an epitaxial growth (Cerutti et al., 2010; Liebich et al., 2010;

Razeghi et al., 1988; Sugo et al., 1990), benzocyclobutene (BCB) polymer bonding (Roelkens et al., 2006), and low-temperature oxygen plasma-assisted bonding (Fang et al., 2006). Facet-free lasers evanescently coupled with Si waveguides were demonstrated for monolithic integration on SOI wafers (Fang et al., 2007, 2008; Liang et al., 2009). However, since the threshold current of these lasers was similar to that of conventional double-heterostructure (DH) lasers, namely a few tens mA, they are not suitable for a low energy operation of 100 fJ/bit or the less. For this purpose an extremely low threshold current operation as well as high-speed modulation capability is required; hence, semiconductor lasers with very small volume of the active region and high-reflectivity mirrors (high Q cavities), such as VCSELs (Iga, 2000), microdisk lasers (Fujita et al., 2000; Spuesens et al., 2009; Van Campenhout et al., 2007, 2009), and photonic crystal (PC) lasers (Jeong et al., 2013; Matsuo et al., 2010; Park et al., 2004; Takeda et al., 2013), can be possible candidates. An extremely low threshold current even below 10 μA was demonstrated in VCSELs and PC lasers.

We proposed a new kind of semiconductor lasers, namely, membrane distributed feedback (DFB) lasers, which consist of a thin semiconductor core sandwiched by low refractive index cladding layers so as to enhance an optical confinement factor of the active region by a factor of around 3 compared with that of conventional DH lasers, and demonstrated very low threshold operation under an optical pump in 2001 (Okamoto et al., 2002). Various studies of membrane DFB lasers operating under an optical pump have been reported (Naitoh et al., 2007; Okamoto et al., 2003, 2004; Sakamoto et al., 2005, 2007a,b,c). Since very low threshold current operation is essentially required for light sources of on-chip optical interconnects, we introduced a lateral current injection (LCI) structure (Oe et al., 1994) into membrane DFB lasers by direct bonding on an SOI substrate (Maruyama et al., 2006; Okumura et al., 2007, 2009, 2011) and by growth on a semi-insulating InP substrate (Okumura et al., 2010; Shindo et al., 2011a,b, 2013a,b). Even though the latter devices showed threshold current similar to that of conventional DH lasers because the optical confinement factor into the active region is not enhanced, an internal quantum efficiency, η_i, of 70% and a waveguide loss, α_{WG}, of 3.5 cm^{-1} were obtained with Fabry–Pérot cavity lasers (Futami et al., 2012). Relatively low threshold current operation (0.23 mA) was obtained with a membrane DFB laser bonded with BCB on an SOI substrate, but its differential quantum efficiency for an output from the front side, η_{df}, was poor (5%) (Inoue et al., 2015).

Then, it was increased by introducing a distributed reflector (DR) structure consisting of a DFB section integrated with high-reflectivity distributed Bragg reflector (DBR) section (Hiratani et al., 2015b).

In this chapter, theoretical and experimental characteristics of LCI-type membrane DFB and DR lasers intended for ultra-low power consumption optical communication systems such as on-chip optical interconnections are presented. Fig. 1 shows a conceptual diagram of the membrane photonic integrated circuit on Si-LSI. First, fundamentals of the membrane laser such as an enhancement of the optical confinement factor of the active region and its effect on threshold current and modulation speed are discussed in Section 2. Then energy cost analysis of the membrane DR laser is discussed in Section 3. Fabrication and static and dynamic lasing characteristics of membrane lasers are given in Section 4. Sections 5 and 6 are devoted for membrane PDs and an integration of the membrane DFB laser with the p-i-n PD, respectively.

2. SEMICONDUCTOR MEMBRANE LASERS FOR LOW POWER OPERATION

Fig. 2 indicates conceptual cross-sectional structures and fundamental mode profiles of a conventional semiconductor laser and a membrane laser. Since the optical mode field of the membrane laser is compressed into thinner region by a high index-contrast ($\Delta n \sim 40\%$) waveguide structure, an optical confinement factor of the active region, ξ, of the membrane laser is approximately three times higher than that of conventional structure. This enhancement allows to increase the modal gain in the membrane laser and

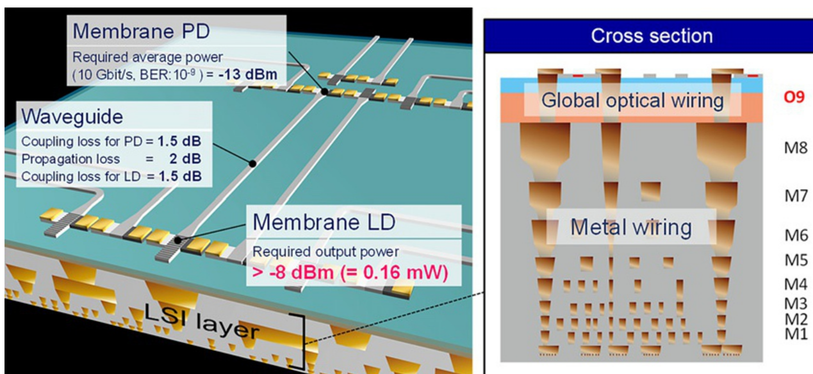

Fig. 1 Image of membrane photonic integrated circuit (MPIC) on a Si-LSI.

will lead to higher modal gain at a fixed injection carrier density or to low threshold current operation when a short cavity structure is adopted. Not only by the enhancement of the modal gain but also by an enhancement of an index-coupling coefficient of the grating in DFB and DBR structures, the active section length of DFB and DR lasers can be shortened to approximately 1/10 times of conventional ones with the same grating depth.

Fig. 3 shows the calculated optical confinement factor of the active region of a slab waveguide in various quantum wells (QWs) as a function

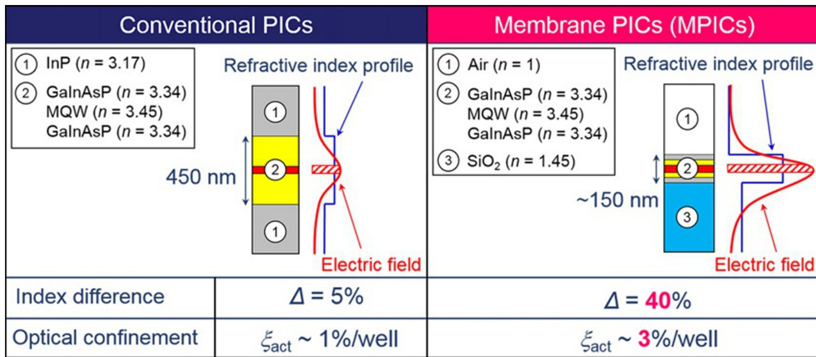

Fig. 2 Comparison of the optical confinement between conventional double-heterostructure laser and membrane laser.

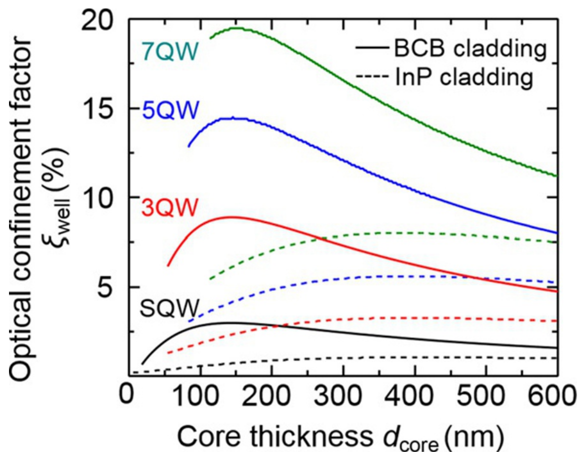

Fig. 3 Optical confinement factor of membrane lasers sandwiched by BCB (*solid lines*) as a function of the semiconductor core thickness. *Dashed lines* indicate that for conventional double-heterostructure sandwiched by InP cladding layers.

of the thickness of the semiconductor core, d_{core} (Okumura et al., 2011). Here, each QW is assumed to consist of 6-nm-thick GaInAsP ($n=3.54$) and 10-nm-thick GaInAsP ($n=3.34$) barriers. As indicated by the solid lines, ξ reaches a maximum value of around 3%/well at d_{core} of around 150 nm and gradually reduces with an increase of d_{core}, whereas that of conventional lasers increases with d_{core} and saturates at around 1%/well.

The enhancement of the optical confinement factor of the membrane laser is very effective not only for reduction of threshold current but also for an increase of direct modulation speed. The relaxation oscillation frequency, f_r, of directly modulated semiconductor laser can be expressed by the following relation:

$$f_r = \frac{1}{2\pi}\sqrt{\frac{\xi G' \eta_i}{eV_a}(I_b - I_{th})} = \frac{1}{2\pi}\sqrt{\frac{\xi (dg/dN) v_g \eta_i}{eV_a}(I_b - I_{th})}, \quad (1)$$

where G' is the differential gain per unit time, g is the medium gain coefficient, N is the injected carrier density, v_g is the group velocity, η_i is the internal quantum efficiency, e is the electronic charge unit, V_a is the volume of the active region, and I_b and I_{th} are the bias current and the threshold current, respectively. The modulation current efficiency (MCEF) can be given by

$$\text{MCEF} = \frac{f_r}{\sqrt{(I_b - I_{th})}} = \frac{1}{2\pi}\sqrt{\frac{\xi (dg/dN) v_g \eta_i}{eV_a}}. \quad (2)$$

For a low energy cost operation of semiconductor lasers, the increase of MCEF by the increase of ξ and the reduction of V_a is required.

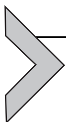

3. ENERGY COST ANALYSIS OF MEMBRANE DR LASERS

In this section, some important results for an energy cost analysis of the membrane DR laser are shown (Hiratani et al., 2015a). By using DFB section length dependences of a threshold current, I_{th}, a differential quantum efficiency for the front side output, η_{df}, the required bias current was calculated for the ultra-low power consumption operation with a high-speed direct modulation of the LCI-membrane DR laser. As mentioned before, a light output power of 0.16 mW at a modulation speed of 10 Gb/s is required by the light source of the on-chip optical interconnection.

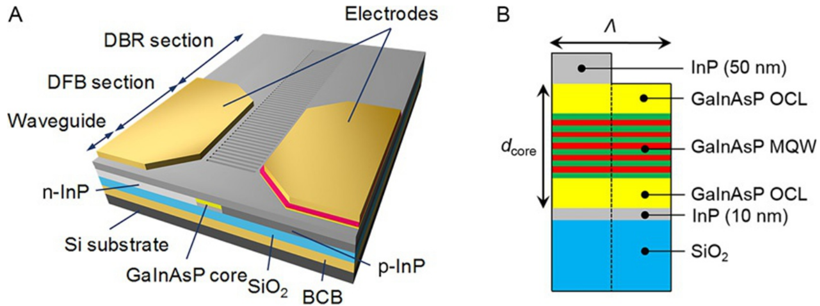

Fig. 4 Schematic structure of (A) a membrane DR laser used for energy cost analysis and (B) its cross-sectional structure of the DFB section.

We assumed that a 3 dB bandwidth f_{3dB} of 7.7 GHz is required for a bit rate of 10 Gb/s, as the bit rate is 1.3 times higher than the f_{3dB} in the nonreturn-to-zero (NRZ) signals.

Fig. 4A and B shows a schematic structure of the LCI-membrane DR laser and its cross-sectional structure, respectively, used for the energy cost analysis, where the active region consists of strain-compensated 5-quantum-well (5QW) and a surface grating with a $\lambda/4$ phase-shift region set at the position of $0.3L_{DFB}$ (L_{DFB} is the length of the DFB section) from the boundary between the DFB and DBR sections because the lower threshold current as well as higher external differential quantum efficiency can be obtained by this $\lambda/4$ phase-shift region.

By varying the index-coupling coefficient, κ_i, of the grating in the DFB section and its length, required input power, P_{in}, to the DR laser was calculated for satisfying the condition of the modulation speed of 10 Gb/s (f_{3dB} of 7.7 GHz) as indicated by open squares in Fig. 5. Here the distance between the active region and p-electrode and the doping concentration of p-InP side cladding layer were assumed to be 1.2 μm and $N_A = 4 \times 10^{18}\,\text{cm}^{-3}$, respectively, and the sheet resistance of it was assumed to be $0.035\,\Omega\,\text{cm}$ for the membrane thickness of 150 nm. Whereas a shorter DFB section (i.e., smaller active region volume) with higher κ leads to lower threshold current and the total power consumption for high-speed modulation can be monotonically reduced as indicated by squares, the total power consumption for the light output power of 0.16 mW becomes much higher for $L_{DFB} < 50$ μm and it reaches a minimum at a certain length of L_{DFB} because an increase of the power consumption in the device resistance (Joule heating power) becomes dominant in very short DFB section length as indicated by painted circles. Therefore, the total power consumption satisfying the both conditions can be higher value for a certain value of L_{DFB}.

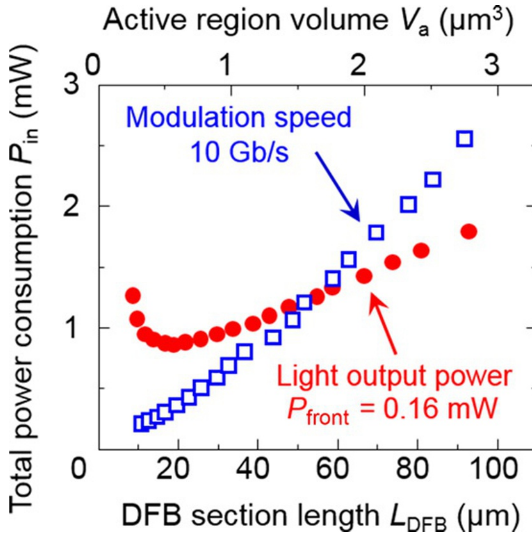

Fig. 5 Total power consumption for the required light output power and that for 10 Gb/s operation as a function of the DFB section length. *From Hiratani, T., Shindo, T., Kyohei Doi, Atsuji, Y., Inoue, D., Amemiya, T., Nishiyama, N., Arai, S., 2015. Energy cost analysis of membrane distributed-reflector lasers for on-chip optical interconnects. IEEE J. Sel. Top. Quantum Electron. 21 (6), 299–308.*

An energy cost [J/bit] of the DR laser can be given by the total power consumption [W] divided by the bit rate [bit/s]. Fig. 6 shows the energy cost of the DR laser for 10 Gb/s signal transmission (indicated by painted circles) and the index-coupling coefficient of the DFB grating (indicated by open squares) as a function of the DFB section length. An energy cost of less than 100 fJ/bit is expected for L_{DFB} of less than 40 μm and a minimum energy cost of 63 fJ/bit can be obtained for $L_{DFB} = 12$ μm, where the active region volume of 0.4 μm^3 and κ_i of 2700 cm^{-1}. For a DFB section length of less than 12 μm, although a lower threshold current is obtained with high κ_i, the total power consumption increases due to the Joule heating.

For further reduction of the total power consumption, a reduction of the optical link loss between the light source and the p-i-n PD and a reduction of the minimum receivable optical power of the p-i-n PD will be required. Fig. 7 indicates the link loss dependence of the energy cost of the DR laser for 10 Gb/s signal transmission and required κ_i of the DFB section. Since the required output power of the DR laser can be reduced by the reduction of the link loss, a structure of shorter L_{DFB} (smaller volume of the active region) with higher κ_i can be adopted. When the link loss is reduced from 5 dB to negligibly small, the energy cost can be reduced from 63 to 28 fJ/bit.

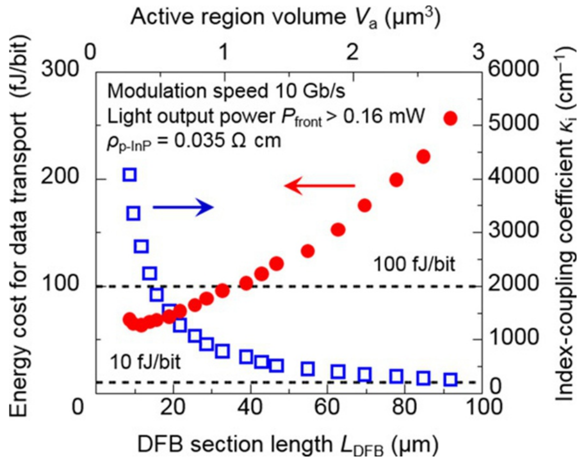

Fig. 6 Energy cost for 10 Gb/s data transport and index-coupling coefficient of an LCI-membrane DR laser as a function of the DFB section length. *From Hiratani, T., Shindo, T., Kyohei Doi, Atsuji, Y., Inoue, D., Amemiya, T., Nishiyama, N., Arai, S., 2015. Energy cost analysis of membrane distributed-reflector lasers for on-chip optical interconnects. IEEE J. Sel. Top. Quantum Electron. 21 (6), 299–308.*

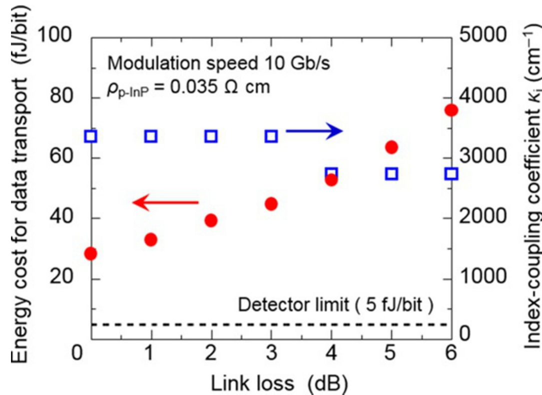

Fig. 7 Minimum energy cost for 10 Gb/s operation and index-coupling coefficient as a function of a link loss. *From Hiratani, T., Shindo, T., Kyohei Doi, Atsuji, Y., Inoue, D., Amemiya, T., Nishiyama, N., Arai, S., 2015. Energy cost analysis of membrane distributed-reflector lasers for on-chip optical interconnects. IEEE J. Sel. Top. Quantum Electron. 21 (6), 299–308.*

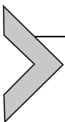

4. MEMBRANE DFB AND DR LASERS ON Si

In this section, after a brief explanation of the fabrication process of membrane DFB and DR lasers bonded on a Si substrate, their typical lasing properties such as static lasing properties and direct modulation properties are explained (Inoue et al., 2015).

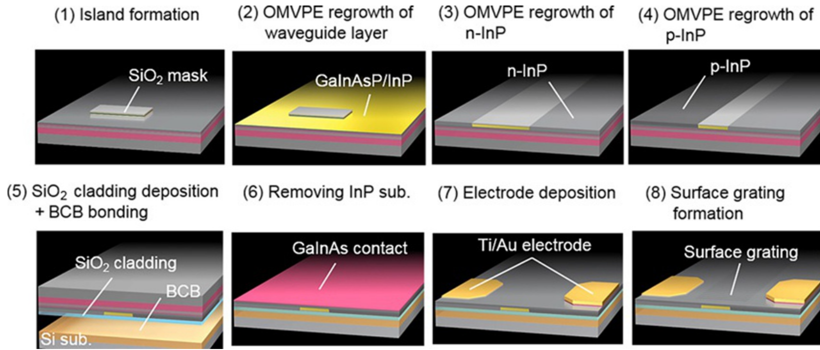

Fig. 8 Fabrication process of a waveguide-integrated LCI-membrane DFB laser. *From Inoue, D., Lee, J., Hiratani, T., Atsuji, Y., Amemiya, T., Nishiyama, N., Arai, S., 2015. Sub-milliampere threshold operation of butt-jointed built-in membrane DFB laser bonded on Si substrate. Opt. Express 23 (6), 7771–7778.*

4.1 Fabrication Process

Fig. 8 shows the fabrication processes of the waveguide-integrated LCI-membrane DFB laser: (1) formation of an island-shaped mesa structure along the [011] direction by CH_4/H_2 reactive-ion etching and selective wet chemical etching, (2) regrowth of GaInAsP waveguide layer for butt-jointed-built-in (BJB) structure by organometallic vapor-phase epitaxy (OMVPE), (3) 7-μm-wide mesa stripe formation and regrowth of an n-InP layer ($N_D = 4 \times 10^{18}\,cm^{-3}$) by OMVPE. After etching one side of the n-InP layer beside the stripe, (4) a p-InP layer ($N_A = 4 \times 10^{18}\,cm^{-3}$) was regrown to form an LCI buried heterostructure with a stripe width of 1–2 μm. Then a 1-μm-thick SiO_2 was deposited onto the wafer by plasma-enhanced chemical vapor deposition followed by (5) the wafer bonding upside-down onto a Si substrate with an intermediate BCB adhesive layer. The BCB layer was prepared by spin coating, followed by curing at 210°C in a N_2 atmosphere. Then, the wafer was bonded to the Si substrate at a pressure of 25 kPa at 130°C. After that, the bonded wafers were baked at 250°C for 1 h in a N_2 atmosphere for hard curing of the BCB adhesive layer. The upper InP substrate side and etch-stop layers were removed by chemical polishing and selective wet chemical etching, thereby revealing the GaInAs contact layer (Fig. 8) (6). After this etching process, the total thickness of the membrane core layers became 270 nm. This contact layer was etched by selective wet etching, except for the p-side electrode region, and the p-InP cap layer on the n-side electrode region was removed to reveal the regrown n-InP layer. Then, (7) Ti/Au electrodes were deposited for both n- and p-type contacts.

Finally, (8) a surface grating structure was formed on the InP cap layer by wet chemical etching with a SiO_2 mask pattern defined by electron-beam lithography. Then, the processed wafer was cleaved into bar form at the waveguide section to measure the light output characteristics. Because the facet had no antireflection coating, the residual reflectivity at the facet is estimated to be approximately 20%.

Fig. 9A shows a scanning electron microscope (SEM) image of the top view of the fabricated waveguide-integrated LCI-membrane DFB laser. Fig. 9B and C shows a schematic diagram of the cross section parallel to the stripe at the coupling section and its SEM image, respectively. Fig. 9D shows an SEM image of the cross section perpendicular to the stripe observed at the passive waveguide section. Although the fabrication process includes a three-step regrowth process, a flat membrane LCI buried heterostructure was successfully obtained.

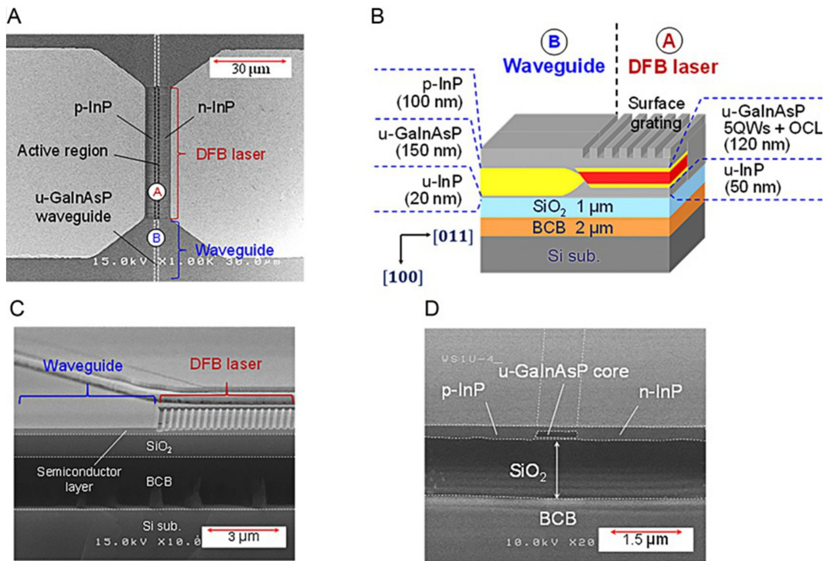

Fig. 9 (A) SEM image of the top view of the fabricated waveguide-integrated LCI-membrane DFB laser. (B) Schematic diagram of the cross section parallel to the stripe at the coupling section. (C) SEM image of the cross section parallel to the stripe observed at the coupling section. (D) SEM image of the cross section perpendicular to the stripe observed at the passive waveguide section. *From Inoue, D., Lee, J., Hiratani, T., Atsuji, Y., Amemiya, T., Nishiyama, N., Arai, S., 2015. Sub-milliampere threshold operation of butt-jointed built-in membrane DFB laser bonded on Si substrate. Opt. Express 23 (6), 7771–7778.*

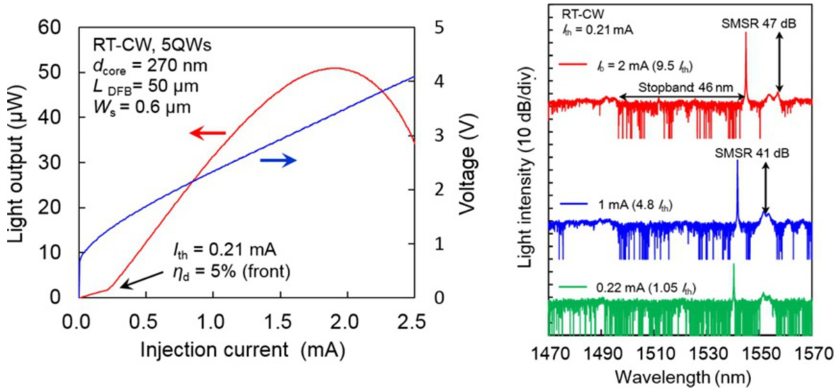

Fig. 10 (A) Light output and voltage–current characteristics of a waveguide-integrated LCI-membrane DFB laser with the DFB section length of 50 µm and the stripe width of 0.6 µm and (B) its lasing spectra at various injection currents. *From Inoue, D., Hiratani, T., Fukuda, K., Tomiyasu, T., Amemiya, T., Nishiyama, N., Arai, S., 2016. Low-bias current 10 Gbit/s direct modulation of GaInAsP/InP membrane DFB laser on silicon. Opt. Express 24 (16), 18571–18579.*

4.2 Static Lasing Properties

Static lasing characteristics of the fabricated membrane DFB laser were measured under RT-CW condition. Fig. 10A shows the light output and the voltage vs injection current characteristics. A threshold current of 0.21 mA and the threshold current density of 700 A/cm^2 (normalized by the number of quantum wells is 140 A/cm^2/well) were obtained with the DFB cavity length of 50 µm and the stripe width of 0.6 µm. An external differential quantum efficiency η_{df} for an output from the front side was only 5%, which may be attributed to the facet phase in respect with the grating period because device had an etched facet without antireflection coating. The operating voltage was reduced to approximately half of that previously reported for the same device length; this can be attributed to the introduction of the alloyed Au/Zn/Au electrode. Fig. 10B shows lasing spectra measured at different bias currents. Stable single-mode operation was observed for a bias current up to 2 mA, after which the light output showed a thermal roll-off. The lasing wavelength was 1542 nm at 1-mA bias current. The side-mode suppression ratio (SMSR) was 41 and 47 dB at bias currents of 1 and 2 mA, respectively. From the lasing spectrum at bias current 2 mA, a stopband width could be determined by measuring the wavelength span where a level of the spontaneous emission intensity was much lower than the noise level of the spectrum analyzer. Based on

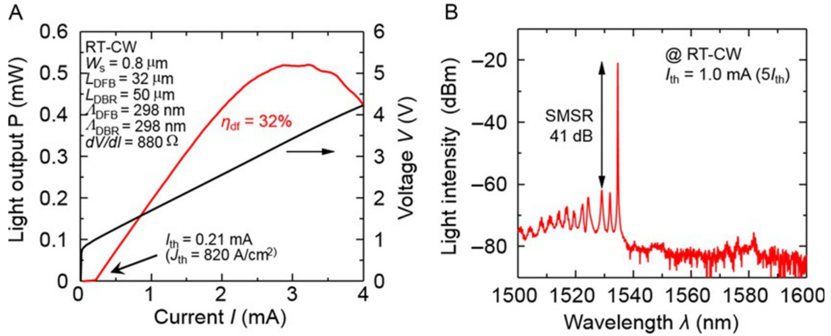

Fig. 11 (A) Light output and voltage–current characteristics of a waveguide-integrated LCI-membrane DR laser with the DFB section length of 50 μm and the stripe width of 0.8 μm and (B) its lasing spectrum at five times the threshold current. *From Tomiyasu, T., Inoue, D., Hiratani, T., Fukuda, K., Nakamura, N., Uryu, T., Amemiya, T., Nishiyama, N., Arai, S., 2018. 20-Gbit/s direct modulation of GaInAsP/InP membrane distributed-reflector laser with energy cost of less than 100 fJ/bit. Appl. Phys. Express 11 (1), 12704.*

the theory of emission spectrum of the DFB laser, the obtained stopband width corresponded to an index-coupling coefficient, κ_i, of 2100 cm^{-1}.

In order to increase the external differential quantum efficiency for the front side output, a membrane DR laser consisting of a DFB section with a DBR at its rear was realized (Tomiyasu et al., 2017). Fig. 11A depicts the current–light and current–voltage characteristics of the device shown in Fig. 4A, under RT-CW operation. The periods of both the DFB and DBR gratings were set to 298 nm, to match the Bragg wavelength in both regions. A threshold current, I_{th}, of 0.21 mA, corresponding to a threshold current density, J_{th}, of 820 A/cm^2, and an external differential quantum efficiency, η_{df}, of 32% for the front side output were obtained. Moreover, the light output from the front side attained a value of 0.16 mW at a bias current of only 0.84 mA. From these curves, a maximum power conversion efficiency of 12.5% was obtained at a bias current of 0.64 mA, and was 12.2% at the bias current of 0.84 mA. The lasing spectrum of the device at a bias current of 1.0 mA (almost five times I_{th}) is shown in Fig. 11B; single-mode operation at 1535 nm with an SMSR of 41 dB was observed. The Bragg wavelength of the DFB section was intentionally not detuned from its gain peak wavelength and the amount of wavelength detuning was estimated to be only 5 nm. The resonant modes in the longer wavelength side of the stopband were not clearly observed because they were approximately 40 nm away from the Bragg wavelength and their optical

gains were considerably low. The index-coupling coefficient, κ_i, is estimated to be approximately $1800\,\text{cm}^{-1}$, from the stopband width of the other devices fabricated at the same time.

4.3 Direct Modulation Properties

The direct modulation characteristics of the DR laser, whose static properties are shown in Fig. 11, were measured based on small-signal modulation response and 20-Gb/s large-signal modulation (Tomiyasu et al., 2018). First, the small-signal response was measured using a vector network analyzer. An electrical modulation signal was applied to the device via a 40-GHz high-speed ground-signal RF probe with a 100-μm pitch. The optical output signal was coupled to a spherical-lensed single-mode fiber. Finally, the collected optical signal was detected by a 20-GHz p-i-n-TIA (transimpedance amplifier) photoreceiver. Since the relaxation oscillation frequency, f_r, measured by relative intensity noise (RIN) has coincided with that by small-signal response measurement, S_{21} for bias currents ranging from 0.46 to 1.21 mA was measured as shown in Fig. 12A. As the bias current was increased up to 1.21 mA, both the relaxation oscillation frequency, f_r, and 3-dB bandwidth, f_{3dB}, increased. At a bias current of 0.77 mA, f_{3dB} reached 11.2 GHz, which implies that not only 10-Gb/s operation but also 15-Gb/s operation can be possible with a bias current of

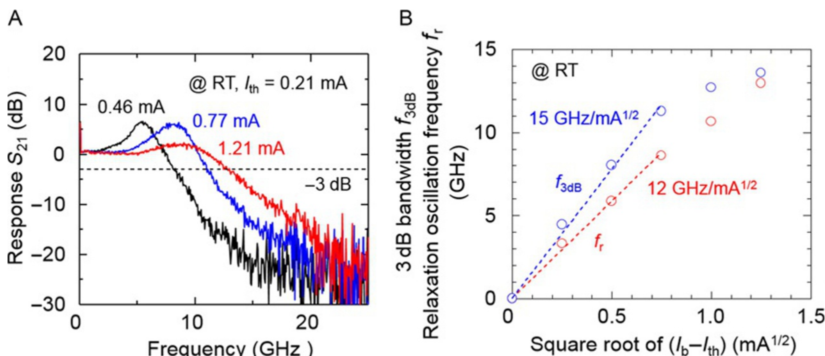

Fig. 12 Small-signal modulation response of the membrane DR laser shown in Fig. 11: (A) responses of S_{21} measured for various bias currents and (B) plots of relaxation oscillation frequency f_r and 3-dB bandwidth f_{3dB} as a function of square root of bias current above threshold. *From Tomiyasu, T., Inoue, D., Hiratani, T., Fukuda, K., Nakamura, N., Uryu, T., Amemiya, T., Nishiyama, N., Arai, S., 2018. 20-Gbit/s direct modulation of GaInAsP/InP membrane distributed-reflector laser with energy cost of less than 100 fJ/bit. Appl. Phys. Express 11 (1), 12704.*

approximately 1.0 mA. The maximum f_{3dB} of 13.6 GHz was obtained at a bias current of 1.77 mA. From the small-signal modulation response, f_r and f_{3dB} were obtained as a function of the square root of bias current above the threshold current, as shown in Fig. 12B. The slopes of f_r (modulation current efficiency factor: MCEF) and f_{3dB} were 12 and 15 GHz/mA$^{1/2}$, respectively.

Finally, 20-Gb/s large-signal direct modulation and bit-error-rate (BER) measurements were performed by using an electrical data signal of the NRZ modulation scheme with a $2^{11}-1$ bit word-length pseudo-random bit sequence generated by an arbitrary waveform generator. The optical output was amplified by an Er-doped fiber amplifier (EDFA), and the amplified spontaneous emission was filtered by a tunable bandpass filter. The amplified optical power was monitored and attenuated by using a variable optical attenuator before the 20-GHz p-i-n-TIA photoreceiver. Fig. 13A shows the BER characteristics of the membrane DR laser at a data rate of 20 Gb/s as a function of average received power. The bias current for the device was set to 1.06 mA. The minimum BER of 6.4×10^{-10} was obtained at an average received power of -4.8 dBm. This result demonstrates the feasibility of the membrane DR laser as a light source with ultra-low power consumption for on-chip optical interconnections. Fig. 13B shows an electrical input

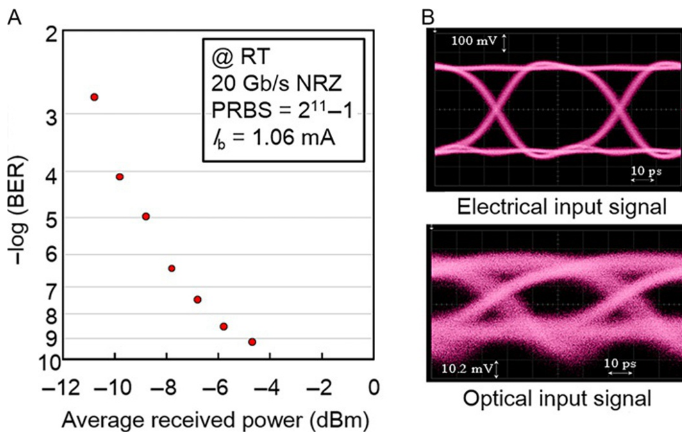

Fig. 13 (A) Measured bit-error-rate (BER) dependence on average received power at 20 Gb/s large-signal modulation and (B) eye diagrams of input electrical signal and optical output measured at a BER of 6.4×10^{-10}. *From Tomiyasu, T., Inoue, D., Hiratani, T., Fukuda, K., Nakamura, N., Uryu, T., Amemiya, T., Nishiyama, N., Arai, S., 2018. 20-Gbit/s direct modulation of GaInAsP/InP membrane distributed-reflector laser with energy cost of less than 100 fJ/bit. Appl. Phys. Express 11 (1), 12704.*

signal and the 20-Gb/s eye diagram measured at an average received power of −4.8 dBm. From a bias voltage of 1.76 V at an injection current of 1.06 mA, the energy cost for this modulation was obtained as 93 fJ/bit; to the best of our knowledge, this is the lowest value reported for membrane DFB and DR lasers. A low energy cost of 97 fJ/bit under 25.8 Gb/s modulation was demonstrated for a similar DR laser bonded on SiO_2/Si substrate, which had a differential resistance of less than 72 Ω and was biased at only 1.04 V (Fujii et al., 2018). If the differential resistance and the bias voltage can be reduced similarly, the energy cost of the DR laser can be further reduced to around 55 fJ/bit (@ 20 Gb/s).

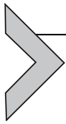

5. MEMBRANE PD ON Si

In this section, after a brief explanation of the fabrication process of membrane DFB and DR lasers bonded on a Si substrate, their typical lasing properties such as static lasing properties and direct modulation properties are explained (Gu et al., 2018).

Fig. 14A shows the schematic structure of the GaInAs/InP p-i-n waveguide-type membrane-based PD bonded on a Si substrate. The device

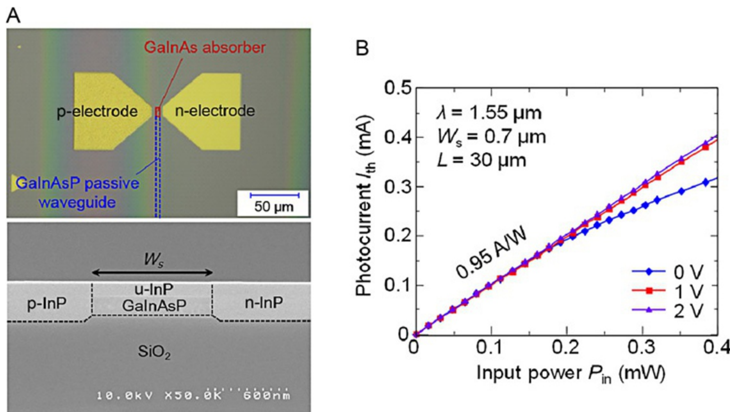

Fig. 14 (A) Structure of a membrane p-i-n photodiode (PD) consisting of absorber region (120-nm-thick GaInAs) integrated with waveguide region (GaInAsP). The stripe width and the absorption region length were 0.7 and 30 μm, respectively. (B) Photocurrent characteristics against input optical power for various applied voltages. *From Gu, Z., Inoue, D., Amemiya, T., Nishiyama, N., Arai, S., 2018. 20 Gbps operation of membrane-based GaInAs/InP waveguide-type p–i–n photodiode bonded on Si substrate. Appl. Phys. Express 11 (2), 22102.*

consisted of a 30-μm-long absorption section with a 120-nm-thick GaInAs bulk layer connected to a passive waveguide section with 155-nm-thick GaInAsP ($\lambda_g = 1.22\,\mu m$) using a BJB structure, and the stripe was 0.7 μm in both sections. Fig. 14B shows the observed photocurrent as a function of input optical power for various applied voltages, where 1.55 μm wavelength TE-polarized light was coupled from a lensed fiber to the membrane PD through the GaInAsP waveguide section. Because the facet of input end was as cleaved without antireflection coating, the coupling efficiency between the lensed fiber to the membrane PD was calculated to be approximately 20%; according to the finite difference method, the responsivity was estimated to be 0.95 A/W.

Fig. 15A shows the BER characteristics of the membrane p-i-n PD for data rates of 10 and 20 Gb/s as a function of average received power, P_{rec}, where NRZ PRBS ($2^7 - 1$) signal and the applied voltage of −3 V were used. The BER of less than 1×10^{-9} was obtained with $P_{rec} = -10$ and −13 dBm for 20 and 10 Gb/s, respectively. As can be seen in Fig. 15B, eye opening was slightly degraded for 20 Gb/s. Much shorter device with smaller capacitance will be required not only for faster operation but also for higher load resistance to increase output voltage.

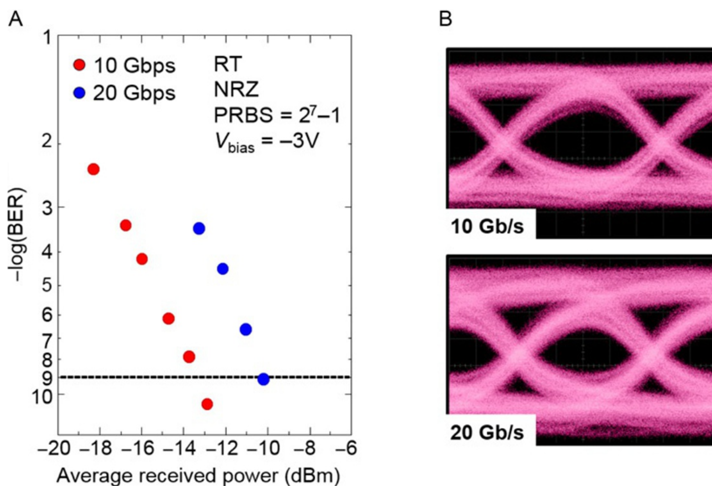

Fig. 15 (A) Measured bit-error-rate (BER) dependences on average received power and (B) eye diagrams for 10 and 20 Gb/s at bias voltage of −3 V. *From Gu, Z., Inoue, D., Amemiya, T., Nishiyama, N., Arai, S., 2018. 20 Gbps operation of membrane-based GaInAs/InP waveguide-type p–i–n photodiode bonded on Si substrate. Appl. Phys. Express 11 (2), 22102.*

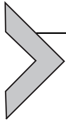

6. INTEGRATED MEMBRANE DFB LASER AND p-i-n PD

In this section, a preliminary optical link consisting of a membrane-based DFB laser integrated with a p–i–n PD prepared on a Si substrate is explained (Inoue et al., 2015). The fabrication process is almost the same as that shown in Fig. 8. Fig. 16A shows an optical microscopic image of the fabricated membrane optical link and cross sections at the active and passive regions. The DFB laser and the p–i–n PD had lengths of 80 and 200 μm, respectively. The absorption layer of the p–i–n PD was the same as that of the active region of the DFB laser. These devices were connected by a 500-μm-long passive waveguide. The coupling efficiency between the active and passive section was calculated to be 98%. The propagation loss of the passive waveguide was measured to be more than 8 dB/cm by the Fabry–Perot resonance method using the waveguide with both cleaved facets. The propagation loss for a 500-μm-long waveguide was at least 0.4 dB. The output of the DFB laser on the opposite side to the p–i–n PD was cleaved, for measuring the lasing characteristics. Fig. 16B shows a scanning electron microscopic image of the DFB laser region. As can be seen, the surface grating pattern was successfully formed on the InP cap layer.

The optical link was then statically characterized, by measuring the optical transmission properties between the DFB laser and the p–i–n PD. Fig. 17A shows the light output of the DFB laser measured by an external

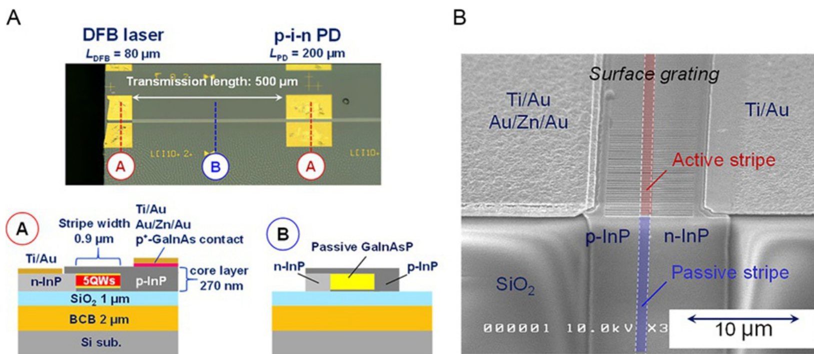

Fig. 16 (A) Optical microscopic image and cross sections of an optical link using a membrane DFB laser and a membrane p-i-n PD. (B) Scanning electron microscopic image of the joint region of the DFB laser and the passive waveguide. *From Inoue, D., Hiratani, T., Fukuda, K., Tomiyasu, T., Gu, Z., Amemiya, T., Nishiyama, N., Arai, S., 2017. Integrated optical link on Si substrate using membrane distributed-feedback laser and p-i-n photodiode. IEEE J. Sel. Top. Quantum Electron. 23 (6), 3700208.*

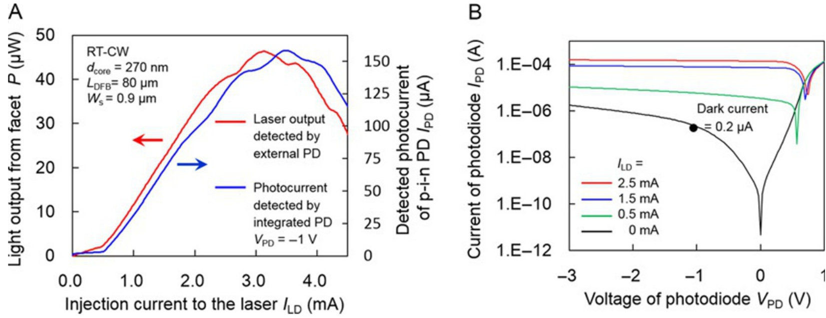

Fig. 17 (A) Photocurrent of the integrated p-i-n PD and light output power of the laser (measured by an external PD) as a function injection current to the laser. (B) Current–voltage characteristics of the integrated p-i-n PD, for various injection currents in the DFB laser. *From Inoue, D., Hiratani, T., Fukuda, K., Tomiyasu, T., Gu, Z., Amemiya, T., Nishiyama, N., Arai, S., 2017. Integrated optical link on Si substrate using membrane distributed-feedback laser and p-i-n photodiode. IEEE J. Sel. Top. Quantum Electron. 23 (6), 3700208.*

PD (on the left) from the opposite side of the p-i-n PD and measured photocurrent, I_{PD}, of the integrated p-i-n PD (on the right), as a function of the injection current, I_{LD}, into the membrane DFB laser. As can be seen, the threshold current of the DFB laser observed from the photocurrent of the integrated p-i-n PD was the same as that measured by the external PD. The slope of I_{LD}–I_{PD} characteristics was 68 μA/mA. Fig. 17B shows the current–voltage characteristics of the integrated p-i-n PD for various injection currents to the membrane DFB laser. The dark current of the p-i-n PD was 0.2 μA at a bias voltage of −1 V, which corresponds to the dark current density normalized by the absorption area of 1×10^{-1} A/cm^2.

Fig. 18A shows the small-signal frequency response (40 MHz to 20 GHz) of the optical link for various injection currents into the membrane DFB laser, with a fixed bias voltage, V_{PD}, of −3 V to the p-i-n PD. A clear relaxation oscillation behavior was observed. In addition, the peak frequency increased with the increase in the DFB laser bias current. Therefore, these responses are not electrical cross-talk between probes, but indeed the transmitted optical signal. The 3-dB bandwidth of the optical link was 11.3 GHz at $I_{LD} = 2.73$ mA. Fig. 18B shows the small-signal response for various bias voltages applied to the p-i-n PD, for $I_{LD} = 2.5$ mA. An increase of the reverse bias voltage enhanced the 3-dB bandwidth which can be attributed to carrier extraction by the applied electric field.

Data transmission via the membrane optical link was performed by large-signal direct modulation of the DFB laser. The input electrical signal

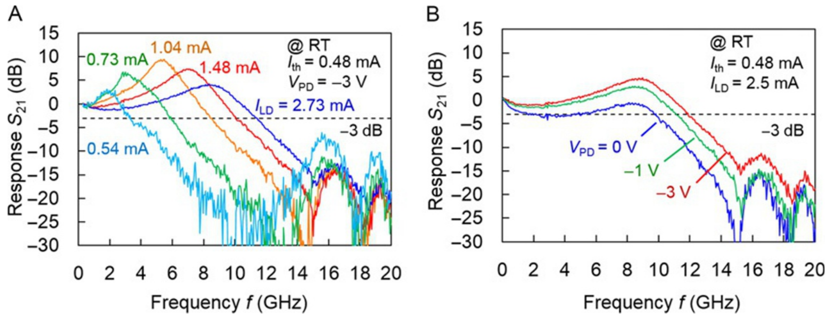

Fig. 18 Small-signal responses of the fabricated optical link; (A) injection current dependence measured at a −3 V bias voltage to the p-i-n PD and (B) bias voltage dependence measured at 2.5 mA injection current of the DFB laser. *From Inoue, D., Hiratani, T., Fukuda, K., Tomiyasu, T., Gu, Z., Amemiya, T., Nishiyama, N., Arai, S., 2017. Integrated optical link on Si substrate using membrane distributed-feedback laser and p-i-n photodiode. IEEE J. Sel. Top. Quantum Electron. 23 (6), 3700208.*

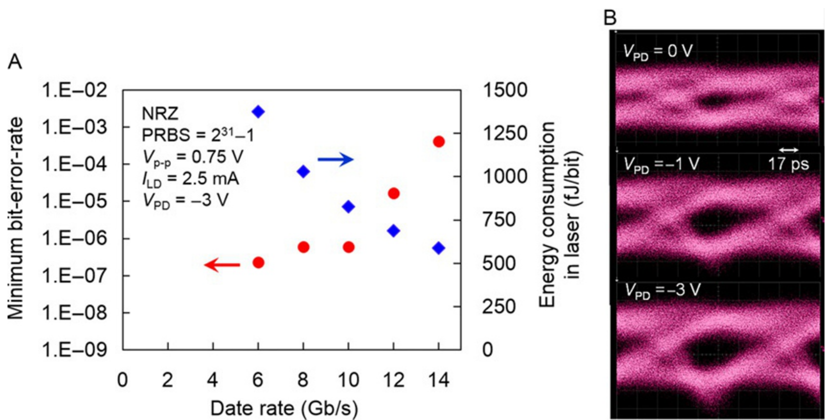

Fig. 19 (A) Bit-error-rate characteristics and energy consumption in the laser of NRZ signal transmission through the membrane optical link, with the laser bias current of 2.5 mA and the p-i-n PD bias voltage of −3 V. (B) 10 Gb/s eye diagrams for the p-i-n PD bias voltages of 0 and −3 V. *From Inoue, D., Hiratani, T., Fukuda, K., Tomiyasu, T., Gu, Z., Amemiya, T., Nishiyama, N., Arai, S., 2017. Integrated optical link on Si substrate using membrane distributed-feedback laser and p-i-n photodiode. IEEE J. Sel. Top. Quantum Electron. 23 (6), 3700208.*

to the DFB laser was NRZ PRBS of $2^{31}-1$ signal, with a voltage swing of 0.75 V_{pp}. Fig. 19A shows the measured BER vs the data rate and the energy consumption in the laser at each data rate. All plots were obtained under the same operating conditions (except for the data rate). A BER in the order of 10^{-7} was obtained up to a data rate of 10 Gb/s. As can be seen

in Fig. 19B, clear eye opening was not obtained for $V_{PD} = 0$ V and it was much improved for $V_{PD} = -3$ V, which is consistent with the result of the small-signal measurements.

Since the optical link demonstrated here consisted of membrane DFB laser and membrane p-i-n PD with the same active and absorber regions, much higher performance can be expected when the membrane DR laser and the membrane p-i-n PD explained in Sections 4 and 5 are combined.

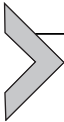

7. SUMMARY

Our recent investigations of semiconductor membrane lasers and PDs intended for on-chip optical interconnection are explained. A high index-contrast thin semiconductor structure, named semiconductor membrane, allows us to reduce the threshold current of membrane DFB and DR lasers without sacrificing the differential quantum efficiency and to enhance the MCEF to more than two times that of conventional semiconductor lasers. As the result, high-speed direct modulation with the injection current of around 1 mA allows us to demonstrate 20 Gb/s modulation with the energy cost of less than 100 fJ/bit. While there is a room for improvement of the energy cost by reductions of the optical link loss (waveguide loss) and the electrical resistance, it can be reduced to around 30 fJ/bit. For further reduction, the minimum receivable optical power of the membrane p-i-n PD will be a key issue.

REFERENCES

Banerjee, K., Mehrotra, A., 2001. Global (interconnect) warming. IEEE Circuits Devices Mag. 17 (5), 16–32.

Binetti, P.R.A., Leijtens, X.J.M., De Vries, T., Oei, Y.S., Di Cioccio, L., Fedeli, J.M., Lagahe, C., Van Campenhout, J., Van Thourhout, D., Van Veldhoven, P.J., Nötzel, R., Smit, M.K., 2010. InP/InGaAs photodetector on SOI photonic circuitry. IEEE Photonics J. 2 (3), 299–305.

Borkar, S., Chien, A.A., 2011. The future of microprocessors. Commun. ACM 54 (5), 67–77.

Cerutti, L., Rodriguez, J.B., Tournie, E., 2010. GaSb-based laser, monolithically grown on silicon substrate, emitting at 1.55 μm at room temperature. IEEE Photonics Technol. Lett. 22 (8), 553–555.

Chen, G., Chen, H., Haurylau, M., Nelson, N.A., Albonesi, D.H., Fauchet, P.M., Friedman, E.G., 2007. Predictions of CMOS compatible on-chip optical interconnect. Integr. VLSI J. 40 (4), 434–446.

Doany, F., 2012. In: Power-efficient, high-bandwidth optical interconnects for high performance computing. IEEE Hot Interconnects Symposium, Santa Clara, CA, August 21–23, 2012.

Fang, A.W., Park, H., Cohen, O., Jones, R., Paniccia, M.J., Bowers, J.E., 2006. Electrically pumped hybrid AlGaInAs-silicon evanescent laser. Opt. Express 14 (20), 9203–9210.
Fang, A.W., Jones, R., Park, H., Cohen, O., Raday, O., Paniccia, M.J., Bowers, J.E., 2007. Integrated AlGaInAs-silicon evanescent race track laser and photodetector. Opt. Express 15 (5), 2315–2322.
Fang, A.W., Lively, E., Kuo, Y.-H., Liang, D., Bowers, J.E., 2008. A distributed feedback silicon evanescent laser. Opt. Express 16 (7), 4413–4419.
Fujii, T., Takeda, K., Diamantopoulos, N.-P., Kanno, E., Hasebe, K., Nishi, H., Nakao, R., Kakitsuka, T., Matsuo, S., 2018. Heterogeneously integrated membrane lasers on Si substrate for low-operating energy optical links. IEEE J. Sel. Top. Quantum Electron. 24 (1), 1500408.
Fujita, M., Ushigome, R., Baba, T., 2000. Continuous wave lasing in GalnAsP microdisk injection laser with threshold current of 40 μA. Electron. Lett. 36 (9), 790–791.
Futami, M., Shindo, T., Koguchi, T., Shinno, K., Amemiya, T., Nishiyama, N., Arai, S., 2012. GaInAsP/InP lateral current injection laser with uniformly distributed quantum-well structure. IEEE Photon. Technol. Lett. 24 (11), 888–890.
Goodman, J., Leonberger, F.I., Kung, S., Athale, R.A., 1984. Optical interconnections for VLSI systems. Proc. IEEE 72 (7), 850–866.
Gu, Z., Inoue, D., Amemiya, T., Nishiyama, N., Arai, S., 2018. 20 Gbps operation of membrane-based GaInAs/InP waveguide-type p–i–n photodiode bonded on Si substrate. Appl. Phys. Express 11 (2), 22102.
Heck, M.J.R., Chen, H.-W., Fang, A.W., Koch, B.R., Liang, D., Park, H., Sysak, M.N., Bowers, J.E., 2011. Hybrid silicon photonics for optical interconnects. IEEE J. Sel. Top. Quantum Electron. 17 (2), 333–346.
Heck, M.J.R., Bauters, J.F., Davenport, M.L., Doylend, J.K., Jain, S., Kurczveil, G., Srinivasan, S., Tang, Y., Bowers, J.E., 2013. Hybrid silicon photonic integrated circuit technology. IEEE J. Sel. Top. Quantum Electron. 19 (4), 6100117.
Hiratani, T., Shindo, T., Doi, K., Atsuji, Y., Inoue, D., Amemiya, T., Nishiyama, N., Arai, S., 2015a. Energy cost analysis of membrane distributed-reflector lasers for on-chip optical interconnects. IEEE J. Sel. Top. Quantum Electron. 21 (6), 299–308.
Hiratani, T., Inoue, D., Tomiyasu, T., Atsuji, Y., Fukuda, K., Amemiya, T., Nishiyama, N., Arai, S., 2015b. Room-temperature continuous-wave operation of membrane distributed-reflector laser. Appl. Phys. Express 8 (11), 112701.
Ho, R., Mai, K., Horowitz, M., 2001. The future of wires. Proc. IEEE 89 (4), 490–504.
Iga, K., 2000. Surface-emitting laser—its birth and generation of new optoelectronics field. IEEE J. Sel. Top. Quantum Electron. 6 (6), 1201–1215.
Inoue, D., Hiratani, T., Atsuji, Y., Tomiyasu, T., Amemiya, T., Nishiyama, N., Arai, S., 2015. Monolithic integration of membrane-based butt-jointed built-in DFB lasers and p-i-n photodiodes bonded on Si substrate. IEEE J. Sel. Top. Quantum Electron. 21 (6), 1502907.
Jeong, K.Y., No, Y.S., Hwang, Y., Kim, K.S., Seo, M.K., Park, H.G., Lee, Y.H., 2013. Electrically driven nanobeam laser. Nat. Commun. 4, 2822.
Kang, Y., Liu, H.D., Morse, M., Paniccia, M.J., Zadka, M., Litski, S., Sarid, G., Pauchard, A., Kuo, Y.H., Chen, H.W., Zaoui, W.S., Bowers, J.E., Beling, A., McIntosh, D.C., Zheng, X., Campbell, J.C., 2009. Monolithic germanium/silicon avalanche photodiodes with 340 GHz gain-bandwidth product. Nat. Photonics 3 (1), 59–63.
Liang, D., Fiorentino, M., Okumura, T., Chang, H.-H., Spencer, D.T., Kuo, Y.-H., Fang, A.W., Dai, D., Beausoleil, R.G., Bowers, J.E., 2009. Electrically-pumped compact hybrid silicon microring lasers for optical interconnects. Opt. Express 17 (22), 20355–20364.

Liao, L., Liu, A., Rubin, D., Basak, J., Chetrit, Y., Nguyen, H., Cohen, R., Izhaky, N., Paniccia, M., 2007. 40 Gbit/s silicon optical modulator for high-speed applications. Electron. Lett. 43 (22), 1196–1197.

Liebich, S., Zimprich, M., Ludewig, P., Beyer, A., Volz, K., Stolz, W., Kunert, B., Hossain, N., Jin, S.R., Sweeney, S.J., 2010. In: MOVPE growth and characterization of Ga(NAsP) laser structures monolithically integrated on Si (001) substrates. Proceedings of the 22nd IEEE International Semiconductor Laser Conference WA5, pp. 143–144.

Liu, J., Sun, X., Kimerling, L.C., Michel, J., 2009. Direct-gap optical gain of Ge on Si at room temperature. Opt. Lett. 34 (11), 1738–1740.

Liu, J., Sun, X., Aguilera, R.C., Kimerling, L.C., Michel, J., 2010. Ge-on-Si laser operating at room temperature. Opt. Lett. 35 (5), 679–681.

Maekawa, T., Ito, H., Masu, K., 2008. In: An 8 Gbps 2.5 mW on-chip pulsed-current-mode transmission line interconnect with a stacked-switch Tx. Proceedings of the 34th European Solid-State Circuits Conference, pp. 474–477.

Manipatruni, S., Chen, L., Lipson, M., 2009. In: 50 Gbit/s wavelength division multiplexing using silicon microring modulators. IEEE International Conference on Group IV Photonics GFP, FC3.

Maruyama, T., Okumura, T., Sakamoto, S., Miura, K., Nishimoto, Y., Arai, S., 2006. GaInAsP/InP membrane BH-DFB lasers directly bonded on SOI substrate. Opt. Express 14 (18), 8184–8188.

Matsuo, S., Shinya, A., Kakitsuka, T., Nozaki, K., Segawa, T., Sato, T., Kawaguchi, Y., Notomi, M., 2010. High-speed ultracompact buried heterostructure photonic-crystal laser with 13 fJ of energy consumed per bit transmitted. Nat. Photonics 4 (9), 648–654.

Mensink, E., Schinkel, D., Klumperink, E., Van Tuijl, E., Nauta, B., 2007. In: A 0.28 pJ/b 2 Gb/s/ch transceiver in 90 nm CMOS for 10 mm on-chip interconnects. IEEE International Solid-State Circuits Conference, pp. 414–416.

Miller, D.A.B., 2000. Rationale and challenges for optical interconnects to electronic chips. Proc. IEEE 88 (6), 728–749.

Miller, D.A.B., 2009. Device requirements for optical interconnects to silicon chips. Proc. IEEE 97 (7), 1166–1185.

Naitoh, H., Sakamoto, S., Ohtake, M., Okumura, T., Maruyama, T., Nishiyama, N., Arai, S., 2007. GaInAsP/InP membrane buried heterostructure distributed feedback laser with air-bridge structure. Jpn. J. Appl. Phys. Part 2 Lett. 46 (47), L1158–L1160.

Oe, K., Noguchi, Y., Caneau, C., 1994. GaInAsP lateral current injection lasers on semi-insulating substrates. IEEE Photonics Technol. Lett. 6 (4), 479–481.

Ohashi, K., Nishi, K., Shimizu, T., Nakada, M., Fujikata, J., Ushida, J., Toru, S., Nose, K., Mizuno, M., Yukawa, H., Kinoshita, M., Suzuki, N., Gomyo, A., Ishi, T., Okamoto, D., Furue, K., Ueno, T., … Akedo, J., 2009. On-chip optical interconnect. Proc. IEEE 97 (7), 1186–1196.

Okamoto, T., Nunoya, N., Onodera, Y., Tamura, S., Arai, S., 2002. Low-threshold singlemode operation of membrane BH-DFB lasers. Electron. Lett. 38 (23), 1444–1446.

Okamoto, T., Nunoya, N., Onodera, Y., Yamazaki, T., Tamura, S., Arai, S., 2003. Optically pumped membrane BH-DFB lasers for low-threshold and single-mode operation. IEEE J. Sel. Top. Quantum Electron. 9 (5), 1361–1366.

Okamoto, T., Yamazaki, T., Sakamoto, S., Tamura, S., Arai, S., 2004. Low-threshold membrane BH-DFB laser arrays with precisely controlled wavelength over a wide range. IEEE Photonics Technol. Lett. 16 (5), 1242–1244.

Okumura, T., Maruyama, T., Kanemaru, M., Sakamoto, S., Arai, S., 2007. Single-mode operation of GaInAsP/InP-membrane distributed feedback lasers bonded on silicon-on-insulator substrate with rib-waveguide structure. Jpn. J. Appl. Phys. 46 (48), l1206–L1208.

Okumura, T., Maruyama, T., Yonezawa, H., Nishiyama, N., Arai, S., 2009. Injection-type GaInAsP-InP-Si distributed-feedback laser directly bonded on silicon-on-insulator substrate. IEEE Photonics Technol. Lett. 21 (5), 283–285.
Okumura, T., Ito, H., Kondo, D., Nishiyama, N., Arai, S., 2010. Continuous wave operation of thin film lateral current injection lasers grown on semi-insulating InP substrate. Jpn. J. Appl. Phys. 49 (4), 40205.
Okumura, T., Koguchi, T., Ito, H., Nishiyama, N., Arai, S., 2011. Injection-type GaInAsP/InP membrane buried heterostructure distributed feedback laser with wire like active regions. Appl. Phys. Express 4 (4), 42101.
Park, H.-G., Kim, S.-H., Kwon, S.-H., Ju, Y.-G., Yang, J.-K., Baek, J.-H., Kim, S.-B., Lee, Y.-H., 2004. Electrically driven single-cell photonic crystal laser. Science 305 (5689), 1444–1447.
Rattner, J., 2006. The Mega-Center. Intel Developer Forum.
Razeghi, M., Defour, M., Blondeau, R., Omnes, F., Maurel, P., Acher, O., Brillouet, F., C-Fan, J.C., Salerno, J., 1988. First cw operation of a $Ga_{0.25}In_{0.75}As_{0.5}P_{0.5}$-InP laser on a silicon substrate. Appl. Phys. Lett. 53 (24), 2389–2390.
Roelkens, G., Van Thourhout, D., Baets, R., Nötzel, R., Smit, M., 2006. Laser emission and photodetection in an InP/InGaAsP layer integrated on and coupled to a silicon-on-insulator waveguide circuit. Opt. Express 14 (18), 8154–8159.
Rong, H., Jones, R., Liu, A., Cohen, O., Hak, D., Fang, A., Paniccia, M., 2005. A continuous-wave Raman silicon laser. Nature 433 (7027), 725–728.
Rong, H., Xu, S., Kuo, Y.H., Sih, V., Cohen, O., Raday, O., Paniccia, M., 2007. Low-threshold continuous-wave Raman silicon laser. Nat. Photonics 1 (4), 232–237.
Rouvìre, M., Vivien, L., Le Roux, X., Mangeney, J., Crozat, P., Hoarau, C., Cassan, E., Pascal, D., Laval, S., F´d´li, J.M., Damlencourt, J.F., Hartmann, J.M., Kolev, S., 2005. Ultrahigh speed germanium-on-silicon-on-insulator photodetectors for 1.31 and 1.55 μm operation. Appl. Phys. Lett. 87 (23), 231109.
Sakamoto, S., Okamoto, T., Yamazaki, T., Tamura, S., Arai, S., 2005. Multiple-wavelength membrane BH-DFB laser arrays. IEEE J. Sel. Top. Quantum Electron. 11 (5), 1174–1179.
Sakamoto, S., Kawashima, H., Naitoh, H., Tamura, S., Maruyama, T., Arai, S., 2007a. Reduced temperature dependence of lasing wavelength in membrane buried heterostructure DFB lasers with polymer cladding layers. IEEE Photonics Technol. Lett. 19 (5), 291–293.
Sakamoto, S., Naitoh, H., Ohtake, M., Nishimoto, Y., Tamura, S., Maruyama, T., Nishiyama, N., Arai, S., 2007b. Strongly index-coupled membrane BH-DFB lasers with surface corrugation grating. IEEE J. Sel. Top. Quantum Electron. 13 (5), 1135–1141.
Sakamoto, S., Naitoh, H., Ohtake, M., Nishimoto, Y., Maruyama, T., Nishiyama, N., Arai, S., 2007c. 85°C continuous-wave operation of GaInAsP/InP-membrane buried heterostructure distributed feedback lasers with polymer cladding layer. Jpn. J. Appl. Phys. 46 (47), L1155–L1157.
Shindo, T., Okumura, T., Ito, H., Koguchi, T., Takahashi, D., Atsumi, Y., Kang, J., Osabe, R., Amemiya, T., Nishiyama, N., Arai, S., 2011a. GaInAsP/InP lateral-current-injection distributed feedback laser with a-Si surface grating. Opt. Express 19 (3), 1884–1891.
Shindo, T., Okumura, T., Ito, H., Koguchi, T., Takahashi, D., Atsumi, Y., Kang, J., Osabe, R., Amemiya, T., Nishiyama, N., Arai, S., 2011b. Lateral-current-injection distributed feedback laser with surface grating structure. IEEE J. Sel. Top. Quantum Electron. 17 (5), 1175–1182.
Shindo, T., Futami, M., Doi, K., Amemiya, T., Nishiyama, N., Arai, S., 2013a. Design of lateral-current-injection-type membrane distributed-feedback lasers for on-chip optical interconnections. IEEE J. Sel. Top. Quantum Electron. 19 (4), 1502009.

Shindo, T., Futami, M., Okumura, T., Osabe, R., Koguchi, T., Amemiya, T., Nishiyama, N., Arai, S., 2013b. Lateral-current-injection type membrane DFB laser with surface grating. IEEE Photonics Technol. Lett. 25 (13), 1282–1285.

Spuesens, T., Liu, L., De Vries, T., Romeo, P.R., Regreny, P., Van Thourhout, D., 2009. In: Improved design of an InP-based microdisk laser heterogeneously integrated with SOI. IEEE International Conference on Group IV Photonics GFP FA3.

Sugo, M., Mori, H., Tachikawa, M., Itoh, Y., Yamamoto, M., 1990. Room-temperature operation of an InGaAsP double-heterostructure laser emitting at 1.55 μm on a Si substrate. Appl. Phys. Lett. 57 (6), 593–595.

Takeda, K., Sato, T., Shinya, A., Nozaki, K., Kobayashi, W., Taniyama, H., Notomi, M., Hasebe, K., Kakitsuka, T., Matsuo, S., 2013. Few-fJ/bit data transmissions using directly modulated lambda-scale embedded active region photonic-crystal lasers. Nat. Photonics 7 (7), 569–575.

Tomiyasu, T., Hiratani, T., Inoue, D., Nakamura, N., Fukuda, K., Uryu, T., Amemiya, T., Nishiyama, N., Arai, S., 2017. High-differential quantum efficiency operation of GaInAsP/InP membrane distributed-reflector laser on Si. Appl. Phys. Express 10 (6), 62702.

Tomiyasu, T., Inoue, D., Hiratani, T., Fukuda, K., Nakamura, N., Uryu, T., Amemiya, T., Nishiyama, N., Arai, S., 2018. 20-Gbit/s direct modulation of GaInAsP/InP membrane distributed-reflector laser with energy cost of less than 100 fJ/bit. Appl. Phys. Express 11 (1), 12704.

TSUBAME2.5, 2013. Hardware Software Specifications. Tokyo Institute of Technology. http://www.gsic.titech.ac.jp/en/node/420.

Van Campenhout, J., Rojo Romeo, P., Regreny, P., Seassal, C., Van Thourhout, D., Verstuyft, S., Di Cioccio, L., Fedeli, J.-M., Lagahe, C., Baets, R., 2007. Electrically pumped InP-based microdisk lasers integrated with a nanophotonic silicon-on-insulator waveguide circuit. Opt. Express 15 (11), 6744–6749.

Van Campenhout, J., Binetti, P.R.A., Romeo, P.R., Regreny, P., Seassal, C., Leijtens, X.J.M., De Vries, T., Oei, Y.S., Van Veldhoven, R.P.J., Nötzel, R., Di Cioccio, L., Fedeli, J.M., Smit, M.K., Van Thourhout, D., Baets, R., 2009. Low-footprint optical interconnect on an SOI chip through heterogeneous integration of InP-based microdisk lasers and microdetectors. IEEE Photonics Technol. Lett. 21 (8), 522–524.

Vivien, L., Osmond, J., Fédéli, J.-M., Marris-Morini, D., Crozat, P., Damlencourt, J.-F., Cassan, E., Lecunff, Y., Laval, S., 2009. 42 GHz pin germanium photodetector integrated in a silicon-on-insulator waveguide. Opt. Express 17 (8), 6252–6257.

Wada, H., Kamijoh, T., 1996. Room-temperature CW operation of InGaAsP lasers on Si fabricated by wafer bonding. IEEE Photonics Technol. Lett. 8 (2), 173–175.

Yang, G.M., MacDougal, M.H., Dapkus, P.D., 1995. Ultralow threshold current vertical-cavity surface-emitting lasers obtained with selective oxidation. Electron. Lett. 31 (11), 886–888.

Yin, T., Cohen, R., Morse, M.M., Sarid, G., Chetrit, Y., Rubin, D., Paniccia, M.J., 2007. 31 GHz Ge n-i-p waveguide photodetectors on silicon-on-insulator substrate. Opt. Express 15 (21), 13965–13971.

Zheng, X., Lexau, J., Luo, Y., Thacker, H., Pinguet, T., Mekis, A., Li, G., Shi, J., Amberg, P., Pinckney, N., Raj, K., Ho, R., Cunningham, J.E., Krishnamoorthy, A.V., 2010. Ultra-low-energy all-CMOS modulator integrated with driver. Opt. Express 18 (3), 3059–3070.